Human Molecular Genetics, 2015, Vol. 24, No. 20 5746–5758

doi: 10.1093/hmg/ddv295
Advance Access Publication Date: 28 July 2015
Original Article

ORIGINAL ARTICLE

Activating the translational repressor 4E-BP or reducing S6K-GSK3β activity prevents accelerated axon growth induced by hyperactive mTOR *in vivo*

Xuan Gong[1,2,3], Longbo Zhang[1,2,3], Tianxiang Huang[1,2,3], Tiffany V. Lin[2,3], Laura Miyares[2,3], John Wen[2,3], Lawrence Hsieh[2,3] and Angélique Bordey[2,3,*]

[1]Department of Neurosurgery, Xiangya Hospital, Central South University, 85 Xiangya Street, Changsha 410008, China, [2]Department of Neurosurgery and [3]Department of Cellular and Molecular Physiology, Yale University School of Medicine, 333 Cedar Street, New Haven, CT 06520-8082, USA

*To whom correspondence should be addressed at: Department of Neurosurgery, Yale University School of Medicine, 333 Cedar Street, FMB 422, New Haven, CT 06520-8082, USA. Tel: +1 2037372515; Fax: +1 2037372159; Email: angelique.bordey@yale.edu

Abstract

Abnormal axonal connectivity and hyperactive mTOR complex 1 (mTORC1) are shared features of several neurological disorders. Hyperactive mTORC1 alters axon length and polarity of hippocampal neurons *in vitro*, but the impact of hyperactive mTORC1 on axon growth *in vivo* and the mechanisms underlying those effects remain unclear. Using *in utero* electroporation during corticogenesis, we show that increasing mTORC1 activity accelerates axon growth without multiple axon formation. This was prevented by counteracting mTORC1 signaling through p70S6Ks (S6K1/2) or eukaryotic initiation factor 4E-binding protein (4E-BP1/2), which both regulate translation. In addition to regulating translational targets, S6K1 indirectly signals through GSK3β, a regulator of axogenesis. Although blocking GSK3β activity did not alter axon growth under physiological conditions *in vivo*, blocking it using a dominant-negative mutant or lithium chloride prevented mTORC1-induced accelerated axon growth. These data reveal the contribution of translational and non-translational downstream effectors such as GSK3β to abnormal axon growth in neurodevelopmental mTORopathies and open new therapeutic options for restoring long-range connectivity.

Introduction

Alterations in long-range cortical connectivity identified using neuroimaging and anatomical methods have been reported in individuals affected by neurodevelopmental disorders associated with hyperactive mTOR complex 1 (mTORC1) (1). Some of the neurological impacts include neurocognitive or psychiatric disorders (2,3) and epilepsy (4). Due to the behavioral importance of altered cortical axon connectivity in mTORC1-related disorders, several studies have examined the impact of hyperactive mTORC1 on axon growth. *In vitro* studies reported that increased mTORC1 activity leads to abnormal axon polarity, namely multiple axons originating from the soma, and increased total axon length (5–7). These studies either expressed a constitutively active form of Rheb, the canonical activator of mTORC1 (8,9), or deleted/knocked down either one of mTORC1's upstream negative regulators *Tsc1* or *Tsc2* (10). In an *in vivo* study, deleting *Tsc1* or knocking down *Tsc2* during corticogenesis resulted in increased axonal coverage of the cortex based on immunostaining for two axonal markers (SMI-31 or SMI-312) (7). In addition, the formation of multiple lateral and basal processes was observed in developing cortical pyramidal neurons in embryonic slice cultures following *Tsc2* knockdown. However, it is not known whether the multiple processes are indicative of multiple axons

Received: April 4, 2015. **Revised:** June 16, 2015. **Accepted:** July 20, 2015

because axonal and dendritic markers were not used. It is thus unclear whether neurons form longer and/or multiple axons *in vivo* in a hyperactive mTORC1 condition during development.

Perhaps even less understood are the mechanisms downstream of mTORC1 regulating axon growth. *In vitro* studies have shown that *Tsc2* knockdown promoted the formation of multiple axons at least in part through SAD kinase (7). Among the downstream targets of mTORC1 are 4E-BP1/4E-BP2 and S6K1/2, which both regulate cap-dependent translation, one of the most studied functions of mTORC1 (11). *In vitro* studies reported that inactivating translation through either constitutive activation of 4E-BP1/2 or knockdown of S6K1/2 was sufficient to prevent axon growth under normal conditions with normal mTORC1 activity (5,6). However, these studies did not examine the contribution of these translational regulators in hyperactive mTORC1 conditions.

We thus set out to determine the impact of hyperactive mTORC1 on axon growth during corticogenesis *in vivo* and examine downstream players with an emphasis on 4E-BPs and S6Ks. To do so, we used *in utero* electroporation to selectively target the anterior cingulate cortex (ACC) and examine axon growth in the contralateral cortex. To increase mTORC1 activity in projection neurons, we transfected cells with a plasmid encoding a constitutively active Rheb ($Rheb^{CA}$) (12–14). This approach allowed us to identify a consistent increase in axon growth in the hyperactive mTORC1 condition and without the formation of multiple axons. We also found that blocking translation by manipulating either 4E-BP1/2 or S6K1/2 was sufficient to prevent mTORC1-induced accelerated axon growth. In addition to translational regulation, S6K1/2 has additional functions through the phosphorylation of several downstream targets (15,16). In particular, hyperactive mTORC1-S6K1 has been shown to directly and indirectly alter the phosphorylation level of GSK3β (17–19), a known regulator of axonal polarity (for reviews, see 20–22). However, it is unknown whether hyperactive mTORC1-S6K1 alters the activity of GSK3β and whether the alteration subsequently contributes to axonal defects. Because of inconsistent experimental effects of GSK3β on normal axon growth *in vitro* and *in vivo* and the level of GSK3β activity under hyperactive mTORC1-S6K1, we examined the level of GSK3β phosphorylation and activity as well as its role in axon growth under normal and hyperactive mTORC1 conditions. We found that GSK3β exhibited increased activity *in vitro* and *in vivo* with hyperactive mTORC1. In addition, blocking GSK3β function *in vivo* prevented the accelerated axon growth induced by hyperactive mTORC1 while having no effect on physiological axon growth.

These data suggest that accelerated axon growth during cortical development can be prevented by either decreasing cap-dependent translation through 4E-BP or reducing GSK3β activity in disorders associated with upregulated tuberous sclerosis complex (TSC)-Rheb-mTORC1 signaling. Remarkably, blocking one of the multiple effectors downstream of mTORC1 is sufficient to prevent abnormal axon growth providing novel strategies to rescue long-range connectivity defects in neurodevelopmental mTORopathies.

Results

Focally increasing mTORC1 activity led to accelerated axon growth without altering neuronal polarity *in vivo*

To examine the impact of increased mTORC1 activity on axonal growth in cortical neurons *in vivo*, we expressed a DNA plasmid encoding $Rheb^{CA}$, the canonical activator of mTORC1, using *in utero* electroporation (Fig. 1A inset). We and others reported that $Rheb^{CA}$ expression allows rapid activation of mTORC1 *in vitro* and *in vivo* (13,14,23,24). We targeted the ACC because this region is routinely affected in individuals with TSC and other neurocognitive disorders (25,26), and it allows for reproducible and accurate axon visualization (Fig. 1A). Electroporation at embryonic day (E) 15 resulted in plasmid expression in Layer 2/3 pyramidal neurons that project axons to the contralateral cortex. The targeted neurons were visualized by cotransfection of a plasmid-expressing tdTomato (Fig. 1A). Following expression of $Rheb^{CA}$ or a control-encoding vector (blue or green fluorescent protein, BFP or GFP) in littermate wild-type mice, visual inspection of tdTomato-fluorescent axons in coronal slices from postnatal day (P) 0 animals revealed that $Rheb^{CA}$ accelerated axon growth (Fig. 1A). Because the number of cells targeted by electroporation is variable, we analyzed sections with equal electroporation efficiency (see Materials and Methods). We found that the length of the longest axons in white and gray matter was significantly increased by 2.5- and 3.6-fold, respectively (statistics and *N* are provided in Fig. 1B and C). In addition, axons had entered the gray matter in the contralateral cortex in only 5/12 of the control mice compared with all of the mice (11/11) in the $Rheb^{CA}$ condition. A gross examination of axonal projections in P3 control versus P0 $Rheb^{CA}$-expressing sections did not reveal obvious targeting differences, but a closer examination would be required to assess whether axon targeting was altered in the $Rheb^{CA}$ condition.

Although hyperactive mTORC1 from either $Rheb^{CA}$ expression or *Tsc2* knockdown has been shown to induce the formation of multiple axons in hippocampal neurons *in vitro* (5–7), we did not find evidence of multiple axons in $Rheb^{CA}$-expressing cortical neurons *in vivo*. We also noted no difference in axon orientation because axons projected in the proper direction, i.e. towards the white matter in both control and $Rheb^{CA}$ condition (Fig. 1D). Processes were identified as axons by ankyrin G immunostaining at P8, and Z-stack imaging was performed to fully examine neurons in three dimensions. The lack of multiple axon formation in $Rheb^{CA}$-expressing neurons was confirmed in 2-month-old animals (Supplementary Material, Fig. S1). Thus, increased mTORC1 activity during development leads to accelerated axon growth without change in polarity (i.e. axon number and direction).

$Rheb^{CA}$-induced accelerated axon growth is rapamycin dependent

$Rheb^{CA}$ can activate mTORC1-independent pathways (23) and has been reported to have mTORC1-independent effects on spines (27). Thus, we tested the effect of the mTORC1 blocker, rapamycin, on the $Rheb^{CA}$-mediated axon elongation. Because rapamycin treatments during embryonic life led to premature birth of the embryos, we tested rapamycin treatments *in vitro*. Cortical neurons were cultured for 4 days following nucleofection with either $Rheb^{CA}$ and tdTomato or BFP and tdTomato (control). Axons were identified by either Tau1 or SMI 312 immunostaining in tdTomato-fluorescent neurons. Neurons transfected with $Rheb^{CA}$ displayed significantly accelerated axon growth compared with those transfected with BFP (Fig. 2A and B). Culturing neurons in the presence of 100 nM rapamycin for 4 days (beginning 4 h after plating) led to a significant decrease in axon length and normalized the length of $Rheb^{CA}$-expressing axons (Fig. 2C and D).

Both 4E-BP1/2 and S6K1/2 contribute to mTORC1-induced accelerated axon growth *in vivo*

Manipulations of either 4E-BP1/2 (constitutive activation) or S6K1/2 (knockdown) have been shown to prevent axon growth

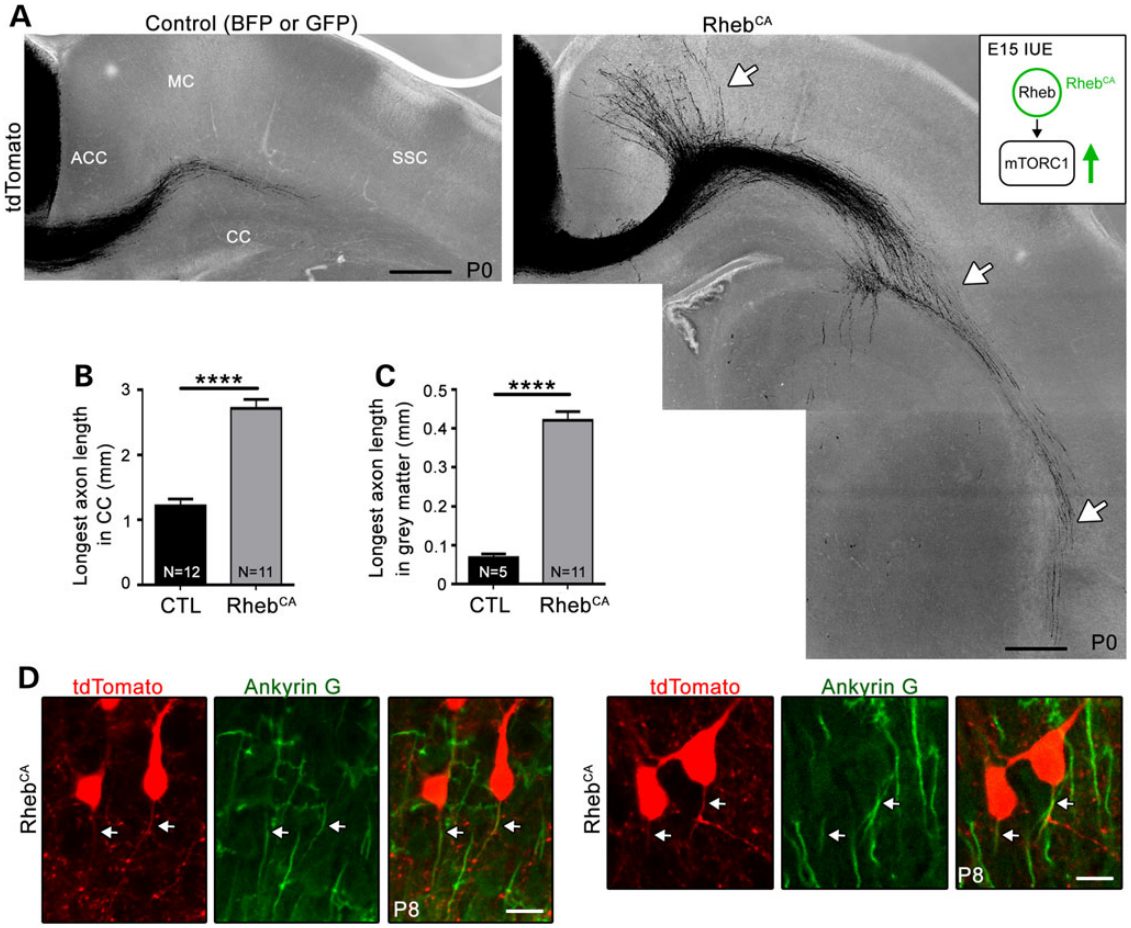

Figure 1. Hyperactive mTORC1 activity accelerates axon growth *in vivo* without affecting polarity. (**A**) Confocal images of tdTomato-fluorescent axonal projections from ACC neurons electroporated at E15 with BFP or GFP [control (CTL), left] or Rheb^{CA} (right). The white arrows point to longer axons in gray and white matter in the Rheb^{CA} condition. CC: corpus callosum, MC: motor cortex, SSC: somatosensory cortex. Inset: diagram illustrating Rheb^{CA} as the canonical activator of mTORC1. IUE = *in utero* electroporation. The green arrow indicates that mTORC1 is hyperactivated following Rheb^{CA} electroporation. Scale bar: 200 μm. (**B** and **C**) Bar graphs of the longest axon length in the corpus callosum (CC, B, $n = 36$ axons in three sections per mouse, $N = 12$ mice in CTL and $n = 33$ axons, 11 mice with Rheb^{CA}) and gray matter (C, $n = 15$ axons, $N = 5$ with CTL and 11 with Rheb^{CA}). Only 5/12 animals display projections into the gray matter in control. Error bars = SEM. N = the number of mice per condition indicated in each column. $^{****}P < 0.0001$ with *t*-test. (**D**) Representative confocal images (Z-stack) of ankyrin G staining in coronal sections containing tdTomato-fluorescent neurons from P8 mice electroporated at E15 with Rheb^{CA}. Scale bar = 30 μm.

under normal conditions *in vitro* (5,6). However, it remains unknown whether manipulating these pathways is sufficient to prevent accelerated growth under hyperactive mTORC1 condition considering the many molecular targets of mTORC1.

To explore the contribution of 4E-BPs, we employed an mTOR-resistant, constitutively active 4E-BP1 plasmid (4E-BP1^{CA}) (Fig. 3A), which constitutively binds eukaryotic initiation factor 4E and therefore mimics the effects of all endogenous 4E-BPs (28). We have previously used this 4E-BP1^{CA} plasmid and reported that it normalizes cap-dependent translation induced by hyperactive mTORC1 *in vitro* and *in vivo* in a different system without affecting S6K1/2 activity (14). Nucleofection of 4E-BP1^{CA} in cortical neurons *in vitro* significantly reduced axon growth on its own and normalized axon length when coexpressed with Rheb^{CA} (Fig. 3B). Coelectroporation of 4E-BP1^{CA} with Rheb^{CA} prevented accelerated axon growth induced by hyperactive mTORC1 *in vivo* (Fig. 3C–E).

To assess the role of S6K1/2, we used a dominant-negative S6K1 (S6K1^{DN}, K100R; 29) *in vitro*, and we also knocked down S6K1/S6K2 using a vector expressing an shRNA against both S6K1 and S6K2 *in vivo* (Fig. 4A). The S6K1^{DN} vector was validated in Neuro2a cells, in which S6K1^{DN} transfection significantly decreased the level of phosphorylated S6 (Ser240/244) (Supplementary Material, Fig. S2). We previously validated this shRNA both *in vivo* and *in vitro* (14). Coelectroporation of S6K1^{DN} with Rheb^{CA} normalized axon length *in vitro* (Fig. 4B). Similarly, coelectroporation of S6K1/2 shRNA with Rheb^{CA} fully normalizes accelerated axon growth induced by hyperactive mTORC1 *in vivo* (Fig. 4C–E).

Collectively, these data suggest that enhancing 4E-BP1/2 activity or blocking S6K1/2 activity *in vivo* is sufficient to normalize accelerated axon growth caused by hyperactive mTORC1. Considering that 4E-BP1/2 is only known to act as a cap-dependent translational repressor, these data suggest that increased cap-dependent translation is necessary for allowing accelerated axon growth induced by hyperactive mTORC1. On the other hand, in addition to regulating translation, S6K1/2 phosphorylates and thus regulates the activity of many targets involved in other cellular processes. One of these downstream pathways, which signals to the well-known regulator of axon development GSK3β, is explored in the next section.

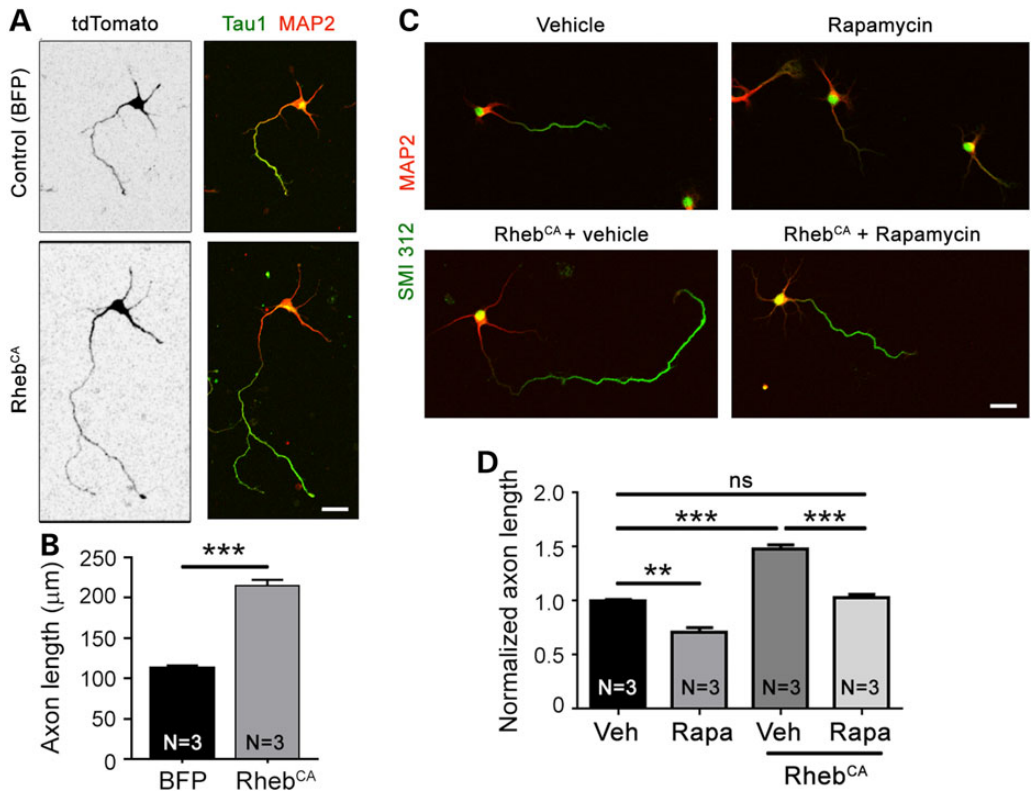

Figure 2. The pharmacological blocker rapamycin prevents increased axon length induced by Rheb^{CA} *in vitro*. (**A**) Confocal images of cortical neurons nucleofected with tdTomato with BFP (control) or Rheb^{CA} at the time of plating and immunostained for Tau1 (green) and MAP2 (pseudocolored red) following 4 days *in vitro*. Scale bar: 20 μm. (**B**) Bar graph of axon length (μm) in neurons nucleofected with either BFP or Rheb^{CA}. *N* = number of neuronal cultures. ***$P < 0.001$ with Student's *t*-test. We measured >130 axons (=cells) per culture and a mean of 522 and 400 axons in the BFP and Rheb^{CA} conditions, respectively, using three sets of culture per condition. (**C**) Confocal images (Z-stack) of cortical neurons nucleofected with tdTomato with BFP (control) or Rheb^{CA} and treated with either vehicle or rapamycin. Scale bar: 20 μm. (**D**) Bar graph of axon lengths (μm) in BFP or Rheb^{CA}-expressing neurons treated with vehicle (Veh) or rapamycin (Rapa). **$P < 0.01$, ***$P < 0.001$ and ns: not significant with one-way ANOVA and Tukey *post hoc* test. We measured more than 45 axons (=cells) per culture and a mean of 213, 352, 162 and 195 axons in the Veh, Rapa, Veh + Rheb^{CA} and Rapa + Rheb^{CA} conditions, respectively, using three sets of culture per condition.

GSK3β activity is increased in hyperactive mTORC1 condition

Hyperactive mTORC1-S6K1/2 is known to indirectly decrease AKT activity and thus GSK3β phosphorylation [at serine (Ser) 9] as part of a negative homeostatic feedback (17,18). Direct phosphorylation of GSK3β by S6K1 has also been reported in *Tsc2* null immortalized cells (19). Thus, to examine GSK3β phosphorylation level in Rheb^{CA} condition, we transfected cortical neurons *in vitro* with Rheb^{CA} or BFP (control) and performed immunoblotting analysis. We found increased phospho-S6 (Ser240/244) and decreased phospho-AKT (Ser473) and phospho-GSK3β (Ser9) in Rheb^{CA}-expressing cortical neurons *in vitro* (Fig. 5B and C). To validate that decreased phospho-GSK3β levels correspond to increased activity, we immunoblotted for the GSK3β target, MAP1B, in Rheb^{CA}-transfected neurons (30,31). Consistent with an increase in GSK3β activity, MAP1B phosphorylation level (Thr1265) was increased in Rheb^{CA}-expressing neurons compared with control (Fig. 5D and E).

To confirm this finding *in vivo*, we used conditional *Tsc1* heterozygous and homozygous knockout mice in which deletion is driven by *Emx1*^{Cre} (*Tsc1*^{cHet} and *Tsc1*^{cKO}) (Supplementary Material, Fig. S3A). In these mice, Cre expression and recombination occurs around E9 in EMX1-positive neural stem cells that generate forebrain glutamatergic neurons and astrocytes. By immunoblotting for readouts of mTORC1 activity (i.e. phospho-S6K1 Thr389 and phospho-S6), we found that the mTORC1 pathway was hyperactive in cortical tissue from P7 *Tsc1*^{cKO} mice. In addition, AKT activity was decreased based on decreased phospho-AKT signal and increased Ser9 GSK3β phosphorylation (Supplementary Material, Fig. S3B and C) as previously reported in different lines of *Tsc1*^{cKO} mice (17,18).

GSK3β does not regulate axon growth during later corticogenesis under physiological condition

GSK3β has been implicated in the regulation of axon growth, but the function of GSK3β on axon growth *in vitro* and *in vivo* remains unclear due to inconsistent findings in previous studies (for reviews, see refs 20–22). We thus examined the impact of either increasing or blocking GSK3β activity on axon growth *in vitro* and *in vivo* using constitutively active and dominant-negative GSK3β mutants (GSK3β^{CA} S9A and GSK3β^{DN} K85M/K86I; 32), which have previously been used by others. We first validated the efficiency of these vectors in Neuro2a cells. In Neuro2a cells, GSK3β^{DN} significantly increased phospho-GSK3β level and decreased phosphorylation of the GSK3β target, CRMP2 (Thr514), indicating decreased GSK3β activity (Supplementary Material, Fig. S4A–C). GSK3β^{CA} had the opposite effect, as expected (Supplementary Material, Fig. S4A–C).

Next, primary cortical neurons were transfected with either GSK3β^{CA} or GSK3β^{DN} and tdTomato. GSK3β^{CA} had no effect on

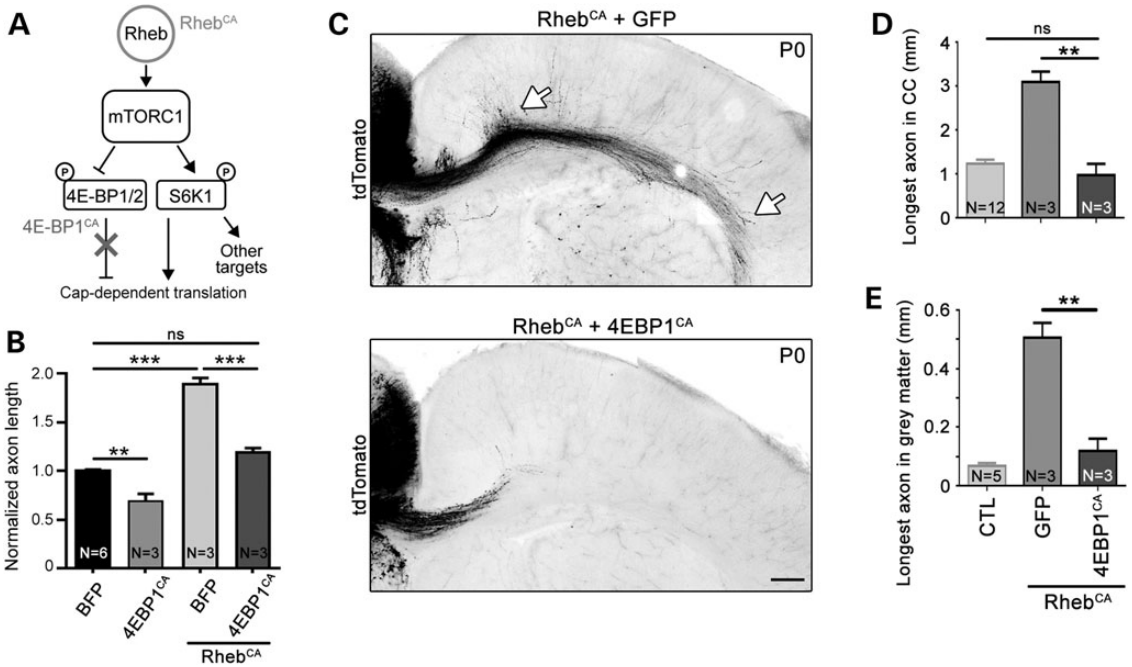

Figure 3. Normalizing cap-dependent translation through 4E-BPs prevents accelerated axon growth induced by hyperactive mTORC1. (**A**) Diagram depicting Rheb-mTORC1 pathway impinging on cap-dependent translation through 4E-BPs and S6Ks. (**B**) Bar graph of axon length (μm) in cultured cortical neurons nucleofected with BFP, 4EBP1^{CA} with and without Rheb^{CA}. *N* = number of neuronal cultures. $^{**}P < 0.01$, $^{***}P < 0.001$ and ns: not significant with one-way ANOVA and Tukey *post hoc* test. We measured >30 axons per culture and a mean of 259, 157, 225 and 322 axons in the BFP, 4EBP^{CA}, BFP + Rheb^{CA} and 4EBP^{CA} + Rheb^{CA} conditions, respectively, using three sets of culture per condition. (**C**) Confocal images of tdTomato-fluorescent axonal projections from ACC neurons electroporated at E15 with Rheb^{CA} + GFP (top) or Rheb^{CA} + 4EBP1^{CA} (bottom). The white arrows point to longer axons in gray and white matter in the Rheb^{CA} condition. Scale bar: 200 μm. (**D** and **E**) Bar graphs of the longest axon length in the corpus callosum (CC, in D, *n* = 6 axons with Rheb^{CA} and 8 axons with Rheb^{CA} + 4EBP1^{CA}, *N* = 3 mice each) and gray matter (in E, *n* = 6 axons in Rheb^{CA} and 6 axons with Rheb^{CA} + 4EBP1^{CA}). Data for the control (CTL: BFP or GFP electroporation only) are those from Figure 1. *N* = the number of mice per condition indicated in each column. $^{**}P < 0.01$ with one-way ANOVA and Tukey *post hoc* test.

axon growth *in vitro*, whereas GSK3β^{DN} decreased axon length by 40% (Fig. 6A and B). *In vivo* neither GSK3β^{CA} nor GSK3β^{DN} had any effect on axon growth (Fig. 6C–E). These data suggest that *in vitro* GSK3β is activated and contributes to axon growth, but additional activation of GSK3β above baseline does not further increase axon growth. *In vivo*, GSK3β does not appear to regulate the elongation of cortical axons as neither vector had any effect on axon length. These *in vivo* data are consistent with those in the GSK3β-S9A knock-in mice (33) and GSK3α-S21A/GSK3β-S9A double knock-in mice as well as in the GSK3β knockout mice that has no axon phenotype (34).

Decreasing GSK3β activity *in vitro* and *in vivo* prevents accelerated axon growth

In light of the effect of GSK3β^{DN} on axon growth *in vitro* and the fact that GSK3β activity is increased in Rheb^{CA} neurons, primary cortical neurons were transfected with GSK3β^{DN} and Rheb^{CA}. GSK3β^{DN} normalized axon length in the hyperactive mTORC1 condition (Fig. 7A and B). These encouraging *in vitro* data led us to test whether blocking GSK3β activity *in vivo* would be sufficient to prevent accelerated axon growth induced by Rheb^{CA}. GSK3β^{DN} was coelectroporated with Rheb^{CA} at E15 and axon length was compared with that in the Rheb^{CA} condition. Visual inspection of axons in P0 coronal sections revealed that GSK3β^{DN} limited accelerated axon growth induced by Rheb^{CA} in both the white and gray matter (Fig. 7C), resulting in a significant reduction in abnormal axon length although not completely back to control level in the gray matter (Fig. 7D and E). We and others previously reported that a focal increase in mTORC1 activity during development leads to neuronal misplacement across cortical layers (35–37). We thus examined placement of Rheb^{CA}-expressing neurons in coronal sections at P8 when migration of electroporated neurons to Layer 2/3 is almost complete. Rheb^{CA} expression at E15 led to cell scattering across cortical layers in coronal sections at P8 as well as the formation of white matter heterotopia (Fig. 7F). GSK3β^{DN} did not prevent neuronal misplacement or white matter heterotopia induced by Rheb^{CA} (Fig. 7F and G). These data highlight a remarkable selectivity for GSK3β in normalizing axon elongation but not neuronal misplacement in hyperactive mTORC1 condition.

Next, we examined whether pharmacologically blocking GSK3β activity *in vitro* and *in vivo* would prevent Rheb^{CA}-induced accelerated axon growth. *In vitro*, we used two well-established pharmacological GSK3β blockers, AR-A014418 and lithium chloride (38,39). In cultured cortical neurons transfected with tdTomato, AR-A014418 (20 μM) and lithium (2 mM) prevented accelerated axon growth in the Rheb^{CA} condition (Fig. 8A–C). Finally, we examined whether LiCl injections *in vivo* (600 mM, every day from E15 to E19, Fig. 8E) would rescue the Rheb^{CA}-induced axonal defect *in vivo*. LiCl significantly prevented the accelerated axon growth in both the gray and white matter (Fig. 8D, F and G).

Discussion

In this study, we focused on determining the function of hyperactive mTORC1 on axon growth during late corticogenesis and identifying downstream players that mediate mTORC1's effects. Our findings are summarized in Figure 9.

Our data reveal that hyperactive mTORC1 during late corticogenesis leads to accelerated axon growth, but hyperactive mTORC1 neurons form one single axon contrary to previous

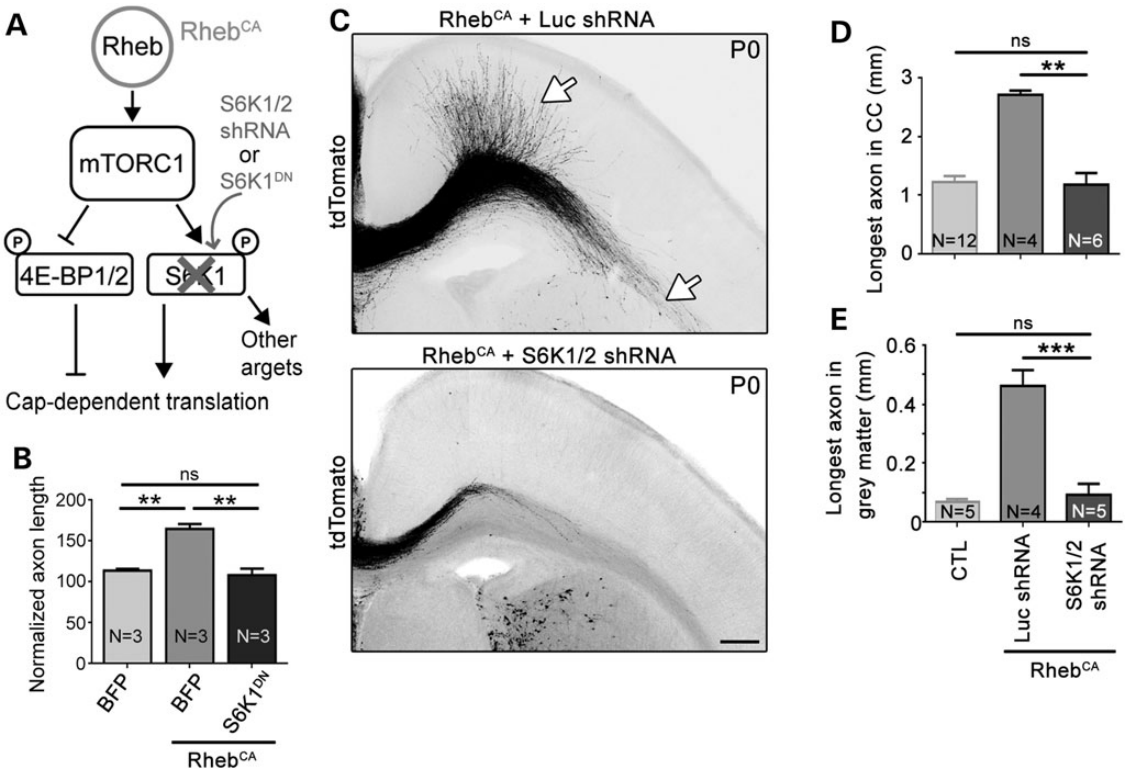

Figure 4. Knocking down S6K1/2 prevents accelerated axon growth induced by hyperactive mTORC1. (**A**) Diagram depicting Rheb-mTORC1 pathway impinging on cap-dependent translation through 4E-BPs and S6Ks. (**B**) Bar graph of axon length (μm) in cultured cortical neurons nucleofected with BFP, S6K1^{DN} with and without Rheb^{CA}. N = number of neuronal cultures. **$P < 0.01$ and ns: not significant with one-way ANOVA and Tukey *post hoc* test. The control condition is the same as that shown in Figure 2B. We measured >29 axons per culture and a mean of 197 and 153 axons in the BFP + Rheb^{CA} and S6K1^{DN} + Rheb^{CA} conditions, respectively, using three sets of culture per condition. (**C**) Confocal images of tdTomato-fluorescent axonal projections from ACC neurons electroporated at E15 with Rheb^{CA} + luciferase (Luc) shRNA or Rheb^{CA} + S6K1/2 shRNA. The white arrows point to longer axons in gray and white matter in the Rheb^{CA} condition. Scale bar: 200 μm. (**D** and **E**) Bar graphs of the longest axon length in the corpus callosum (CC, in D, $n = 10$ axons in Rheb^{CA} + Luc shRNA and $n = 11$ axons in Rheb^{CA} + S6K1/2 shRNA, $N = 4$ mice each) and gray matter (in E, $n = 10$ axons in Rheb^{CA} + Luc shRNA and $n = 11$ axons in Rheb^{CA} + S6K1/2 shRNA, $N = 4$ mice each). Data for the control (CTL, BFP or GFP electroporation only) are those from Figure 1. N = the number of mice per condition indicated in each column. **$P < 0.01$ and ***$P < 0.001$ with one-way ANOVA and Tukey *post hoc* test.

in vitro studies using hippocampal neurons (5–7). An increase in axon length was expected based on previous studies reporting that genetically increasing mTORC1 activity leads to increased axon length *in vitro* and increased axonal tract *in vivo* (7,40). In addition, mTORC1 activation following injury improves axonal regeneration *in vivo* (41–43). The lack of multiple axon formation *in vivo* may be explained by a difference between an *in vitro* and an *in vivo* setting and between regions (hippocampus versus cortex).

Next, in order to identify mTORC1 effectors of axon growth, we focused on 4E-BPs and S6Ks. Coelectroporation of either a constitutively active 4E-BP or an shRNA against S6K1/2 was sufficient to prevent hyperactive mTORC1-induced accelerated axon growth. Considering that 4E-BPs only reported function is the regulation of cap-dependent translation and we previously reported that the 4E-BP1^{CA} vector used here normalized Rheb^{CA}-induced increase in translation *in vivo*, our data suggest that normalizing cap-dependent translation is sufficient to prevent accelerated axon growth in hyperactive mTORC1 condition.

In addition to regulating translation, S6Ks have a multitude of targets (15,16). In particular, under hyperactive mTORC1 condition, S6K1 is part of a negative homeostatic feedback leading to decreased IRS-1 and AKT phosphorylation (for reviews, see 44–46). Consistent with this feedback, two studies using conditional *Tsc1* knockout mice reported decreased AKT phosphorylation resulting in decreased GSK3β S9 phosphorylation (17,18,47). Our data in Rheb^{CA}-expressing neurons *in vitro* as well as conditional *Tsc1*^{cKO} cortex are in agreement with these published data. However, another elegant study suggested that in a *Tsc2* null condition (in immortalized mouse embryonic fibroblasts cells), S6K1 could directly phosphorylate GSK3β and thus lead to hyperphosphorylation of GSK3β (19). The discrepancy between these results is presumably due to the different cell types used. Here, we also found that a GSK3β target, MAP1B, was hyperphosphorylated in Rheb^{CA}-expressing cortical neurons *in vitro* consistent with decreased GSK3β S9 phosphorylation and increased kinase activity.

Considering that GSK3β can regulate axon growth in development (for reviews, see 20–22), we investigated the impact of GSK3β on accelerated axon growth in our system and condition. We first explored the impact of activating or blocking GSK3β activity on normal axon growth because previously published findings have been inconsistent. Indeed, some studies suggest that suppression of GSK3β activity *in vitro* is required for the formation of multiple axons and axon elongation (33,34,48–54), whereas others show that GSK3β inhibition prevents axon extension (52,55–57). To reconcile these inconsistent data, it has been suggested that the final outcome of GSK3β inhibition is dependent on the extent and timing of GSK3β inhibition and the downstream substrates involved (20,51,52). Here, in cultured Rheb^{CA}-expressing cortical neurons, constitutive activation of GSK3β (using a Ser9 to Ala9 substitution in GSK3β) did not alter axon elongation while blocking GSK3β activity with a dominant-negative mutant

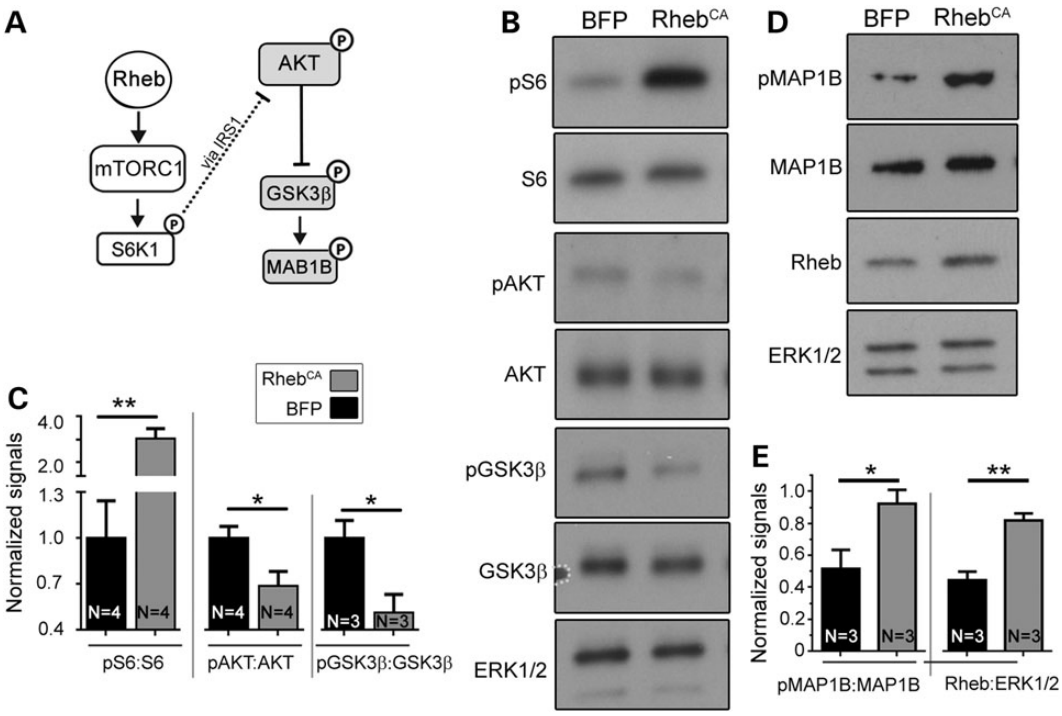

Figure 5. GSK3β activity is increased in Rheb^{CA}-expressing neurons. (**A**) Diagram depicting mTORC1 pathway and the negative feedback from S6K1 indirectly to AKT and GSK3β. (**B**) Western blots for protein indicated on the left of each blot in cortical neurons nucleofected with BFP (control) or Rheb^{CA}. (**C**) Bar graphs of the normalized levels of phospho-(p) S6 over total S6, pAKT over AKT and pGSK3β over GSK3β. (**D**) Western blots for protein indicated on the left of each blot in cortical neurons nucleofected with BFP (control) or Rheb^{CA}. Bar graphs of the normalized levels of pMAP1B over MAP1B and Rheb:ERK1/2. *$P < 0.05$ and **$P < 0.01$ with *t*-test. *N* = number of neuronal cultures.

decreased axon elongation. *In vivo* transgenic mice expressing constitutively active GSK3β and GSK3α (knock-in mice) and GSK3β knockout mice do not display any gross axonal defects (33,34,51). In our condition, neither the constitutively active nor the dominant-negative GSK3β altered axon growth *in vivo* consistent with some findings in previous *in vivo* studies using transgenic mice (33,34). These data suggest that GSK3β activation alone through phosphorylation at Ser9 is not sufficient for altering axon growth and may thus require activation of additional pathways or molecules. Similarly, the lack of effect of blocking GSK3β activity on axon growth during corticogenesis suggests that either GSK3β is not activated or GSK3α compensated for the loss of GSK3β activity. However, data from the Rheb^{CA} condition, in which blocking GSK3β activity is sufficient to prevent accelerated axon growth, suggest that GSK3α is not compensating in this condition. The fact that blocking GSK3β activity does not alter axon growth under normal conditions also suggests that the effect of the dominant-negative GSK3β in the Rheb^{CA} condition is due to normalizing GSK3β activity increased by hyperactive mTORC1.

In conclusion, developing adult cortical neurons expressing hyperactive mTORC1 displayed longer axons and a single axon projecting toward the white matter. The increase in axon length could lead to a premature increase in intercortical axonal connectivity that is expected to impair circuit formation and lead to abnormal network function in adults (58). We also report that blocking GSK3β signaling or cap-dependent translation through 4E-BPs or S6K1/2 in developing neurons limited hyperactive mTORC1-induced accelerated axonal elongation *in vivo*. These data suggest that increased GSK3β activity is required for axon overgrowth *in vivo* in the context of increased mTORC1 activity. Collectively, our findings offer additional molecular targets to limit axonal defects in TSC-mTORC1-related developmental disorders leading to epilepsy and neurocognitive or psychiatric deficits such as TSC and focal cortical dysplasia (59,60) as well as acquired epilepsy associated with mTORC1-dependent axonal sprouting (4).

Materials and Methods

Animals and genotyping

Research protocols were approved by the Yale University Institutional Animal Care and Use Committee. Experiments were performed on wild-type CD1 mice (Charles River Laboratories) for all experiments and R26R^{tdTomato} × *Emx1*^{Cre} × *Tsc1*$^{fl/mut}$ mice (abbreviated *Tsc1*^{cKO}) and *Tsc1*^{cHet} (heterozygous, *Tsc1*$^{fl/wt}$) for preparing cortical lysates for western blot. Both male and female pups were used for experiments. Breeding strategies and genotyping were performed as previously reported (23)

Vectors

Constructs used were as follows: pCAGGS-Rheb^{CA}, human Rheb with S16H mutation, gift from Drs Maehama and Hanada (National Institute of Infectious Diseases, Tokyo) (24); pCAGGS-4EBP1 F113A (i.e. constitutively active 4E-BP1, 4E-BP1^{CA}), synthesized coding sequence for mouse 4EBP1 with F113A mutation inserted into *Eco*RI sites of pCAGGS (14,28); all GSK3β constructs were generated via synthesis of human GSK3β with the appropriate mutations and inserted into pCAG-tdTomato at *Eco*RI and *Not*I, excising tdTomato (pCAG-GSK3β^{DN} with K85M and K86I mutations and pCAG-GSK3β^{CA} with S9A mutation); pCAGGS-S6K1^{DN}, synthesized coding sequence for the α II isoform of mouse S6K1 with K100R mutation cloned into the *Eco*RI sites of pCAGGS; S6K1/S6K2 shRNA (target sequence, CTCAGTGAGAGTGCCAACCAA from 61), inserted into pSicoR (Addgene #12084; 62). pSicoR empty vector was used as the

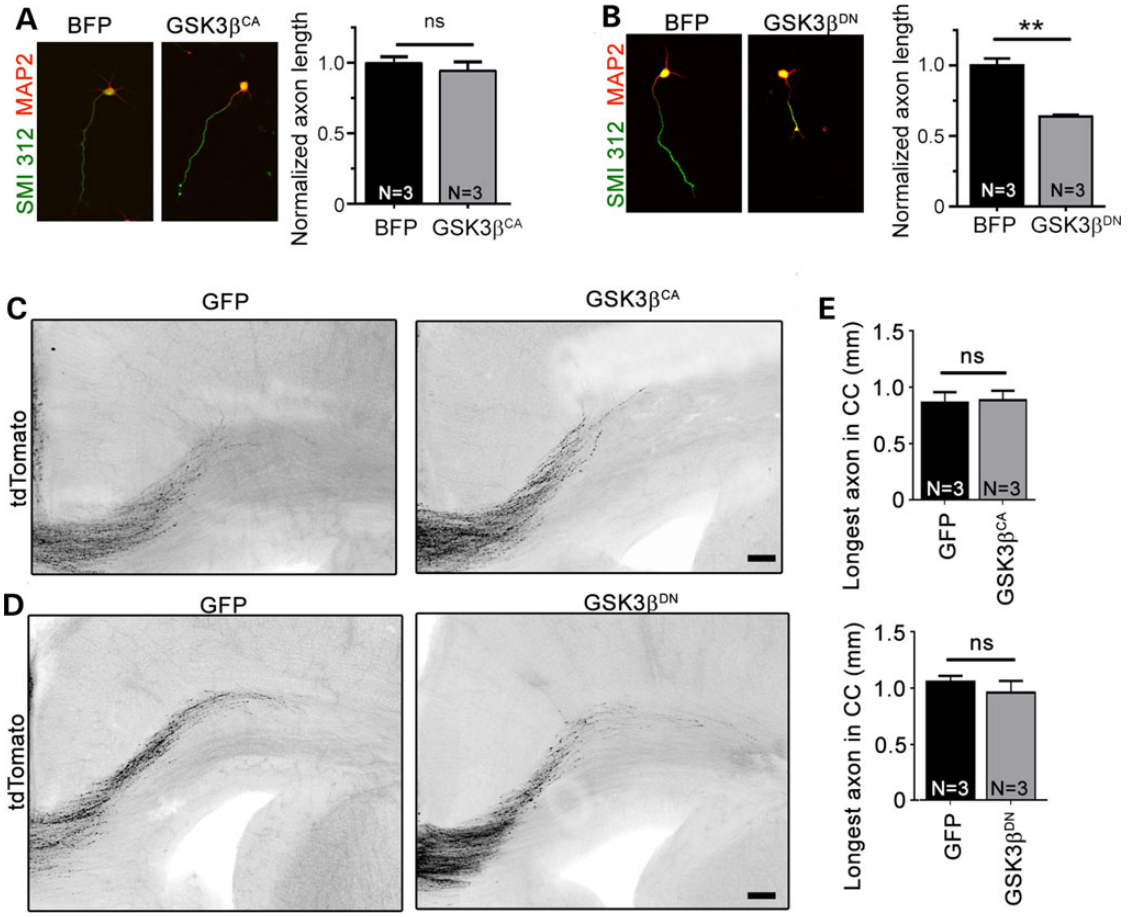

Figure 6. Blocking GSK3β activity decrease axon length *in vitro* but not *in vivo*. (**A** and **B**) Left panels: confocal images of tdTomato-nucleofected (black) cortical neurons cotransfected with BFP, GSK3β^{CA} or GSK3β^{DN} and immunostained for SMI 312 (green) and MAP2 (red). Right panels: bar graphs of axon length under control and GSK3β^{CA} or GSK3β^{DN} conditions. **$P < 0.01$ with Student's *t*-test. N = number of neuronal cultures. We measured >41 axons per culture and a mean of 228, 209 and 240 axons in the BFP, GSK3β^{CA} and GSK3β^{DN} conditions, respectively. (**C** and **D**) Confocal images of tdTomato-fluorescent axonal projections from ACC neurons electroporated at E15 with tdTomato + GFP, GSK3β^{CA} (C) or GSK3β^{DN} (D). Scale bar = 100 μm. (**E**) Bar graphs of the longest axon length in the corpus callosum (CC) under conditions shown under the graph. For GSK3β^{DN} experiment: $n = 12$ axons, $N = 4$ mice in CTL and $n = 8$ axons in GSK3β^{DN}, $N = 3$ mice. For GSK3β^{CA} experiment: $n = 7$ axons in CTL and $n = 8$ axons in GSK3β^{CA}, $N = 3$ mice each.

control for shRNA experiments. pCAG-GFP (Addgene, #11150) and pCAG-BFP (gift from J. Breunig, Cedars Sinai Medical Center) were used as controls for pCAG-GSK3β constructs. Both pCAG-GFP and pCAG-BFP produced similar results in terms of axon length (comparison data not shown). pCAG-tdTomato [tdTomato from pCMV-tdTomato (Clontech) subcloned into pCAG] (63) was used for visualization.

In utero electroporation

Laparotomies were performed on anesthetized, timed pregnant CD-1 mice to gain access to the uterine horns. The lateral ventricles of E15 embryos were injected with plasmids at a concentration of 1–3 μg/μl. DNA constructs were diluted in phosphate buffered saline (PBS) with 0.01% fast green. Tweezertrodes (5 mm, BTX) were used to electroporate the neural progenitors lining the ventricles (five pulses, 50 ms each, 40 V at E15.5).

Brain fixation and immunofluorescence

P0 mouse brains were dissected and drop-fixed in 4% paraformaldehyde overnight before being embedding in 3% agarose. Brains were sectioned coronally at a thickness of 150 μm on a vibratome (Leica VT1000).

For ankyrin G immunostaining, brains of P8 and 2-month-old mice were perfused transcardially with 4% formaldehyde, cryoprotected with 30% sucrose, embedded in optimal cutting temperature compound (Tissue Tek) and sectioned at 100 μm using a microtome. Free-floating sections were incubated for 1 h in a blocking solution (2% bovine serum albumin and 0.3% Triton-X in PBS) at room temperature and then incubated with anti-ankyrin G (NeuroMab, 1:1000) overnight at 4°C. Sections were washed with PBS and then placed in blocking solution containing secondary antibodies (Alexa Fluor conjugated, Molecular Probes, 1:1000) for 1 h at room temperature. All images were taken using an FV1000 confocal microscope (Olympus).

Culture of embryonic cortical neurons followed by nucleofection

The cortices of E16 pups were dissected out, incubated in papain (Worthington) for 15 min at 37°C and dissociated by pipetting in plating medium [minimum essential medium (MEM) supplemented with 5% fetal calf serum, 0.6% glucose, 2 mM glumax]. Following dissociation, cells were nucleofected using a Mouse Neuron Nucleofector kit VPG-1001 (Lonza; 3–5 μg DNA was transfected in 4×10^6 cells following the manufacturer's instructions).

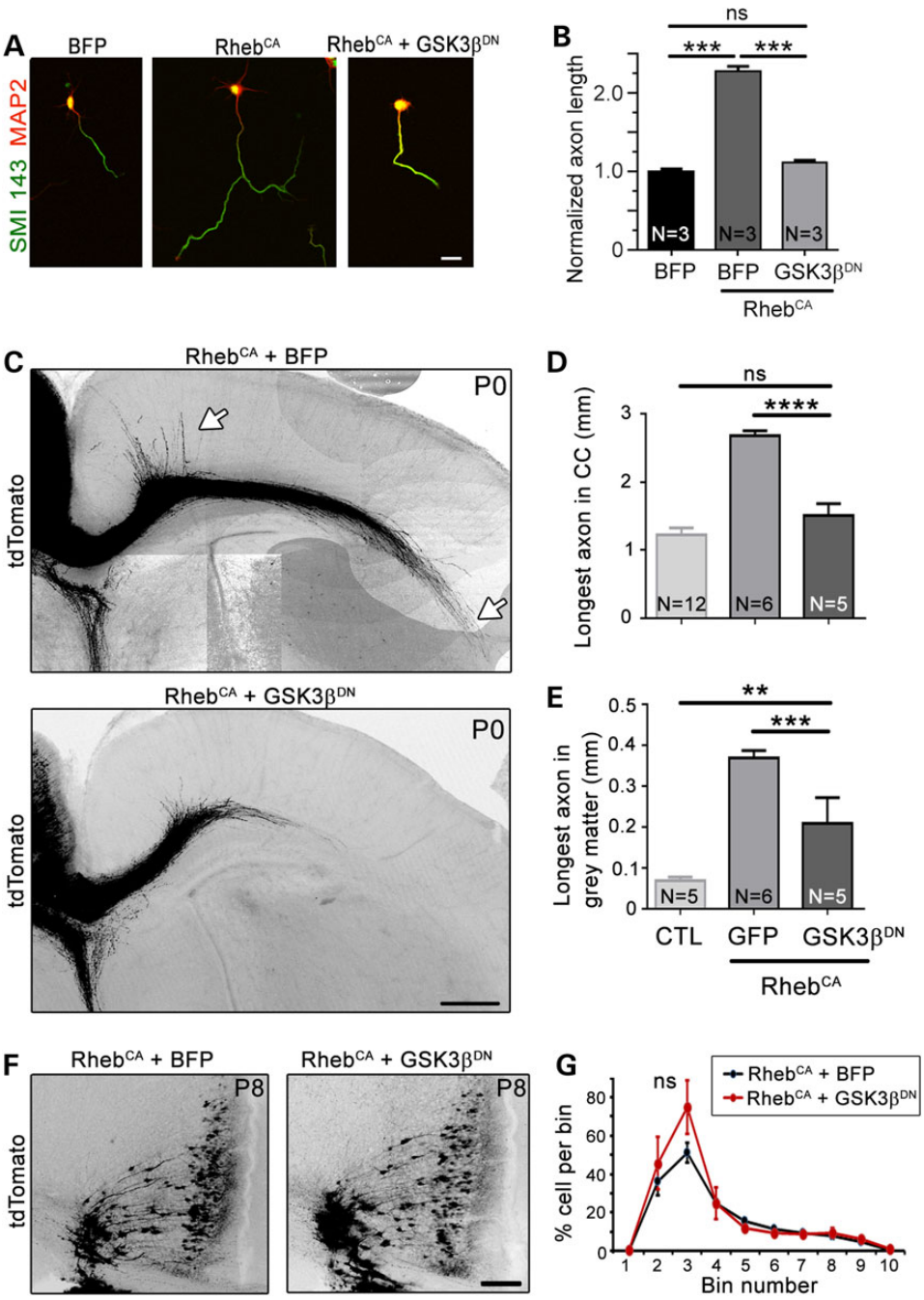

Figure 7. Blocking GSK3β using a dominant-negative vector limits accelerated axon growth *in vitro* and *in vivo*. (**A**) Confocal images of cortical neurons nucleofected with tdTomato with BFP (control), Rheb^{CA} or Rheb^{CA} + GSK3β^{DN} and immunostained for SMI 143 (green) and MAP2 (pseudocolored red). Scale bar = 20 μm. (**B**) Bar graph of axon length (μm) in neurons under conditions shown under the graph. *N* = number of neuronal cultures. ***$P < 0.001$ with one-way ANOVA with Tukey *post hoc* test. We measured >32 axons per culture and a mean of 200, 166 and 180 axons in the BFP, Rheb^{CA} and Rheb^{CA} + GSK3β^{DN} conditions, respectively. (**C**) Confocal images of tdTomato-fluorescent axonal projections from ACC neurons electroporated at E15 with Rheb^{CA} or Rheb^{CA} + GSK3β^{DN}. The white arrows point to longer axons in gray and white matter in the Rheb^{CA} condition. Scale bar = 200 μm. (**D** and **E**) Bar graphs of the longest axon length in the corpus callosum (CC, $n = 17$ axons, $N = 6$ mice in Rheb^{CA} and $n = 13$ axons, $N = 5$ mice in Rheb^{CA} + GSK3β^{DN}) and gray matter (same *n*). *N* = the number of mice per condition indicated in each column. **$P < 0.01$ and ***$P < 0.001$, ****$P < 0.0001$ with one-way ANOVA and Tukey *post hoc* test. Data for the control (CTL, BFP or GFP electroporation only) are those from Figure 1. (**F**) Confocal images of ACC tdTomato-positive neurons in a P8 coronal section electroporated at E15 with either Rheb^{CA} (left) or Rheb^{CA} + GSK3β^{DN} (right). (**G**) Percentage of tdTomato-positive cells counted in the ACC divided into 10 equally (vertically separated) bins with Rheb^{CA} (black) and Rheb^{CA} + GSK3β^{DN} condition (red). ns: not significant with two-way repeated-measures ANOVA.

Cells were then resuspended in MEM supplemented with 0.6% glucose and 5% fetal bovine serum and plated on poly-D-lysine-coated coverslips. The medium was changed to neuronal maintenance media (neurobasal medium with 1× B27 and 1× GlutaMAX-1) 1–2 h after plating. Half of the medium was then changed every 3 days. Neurons were plated at a higher density (1×10^6 cells per well) for western blot and lower density (30–50 000 cells per coverslip) for immunostaining. Western blot and immunostaining were performed 6 and 4 days after plating, respectively. Neurons cultured on coverslips were fixed using 4%

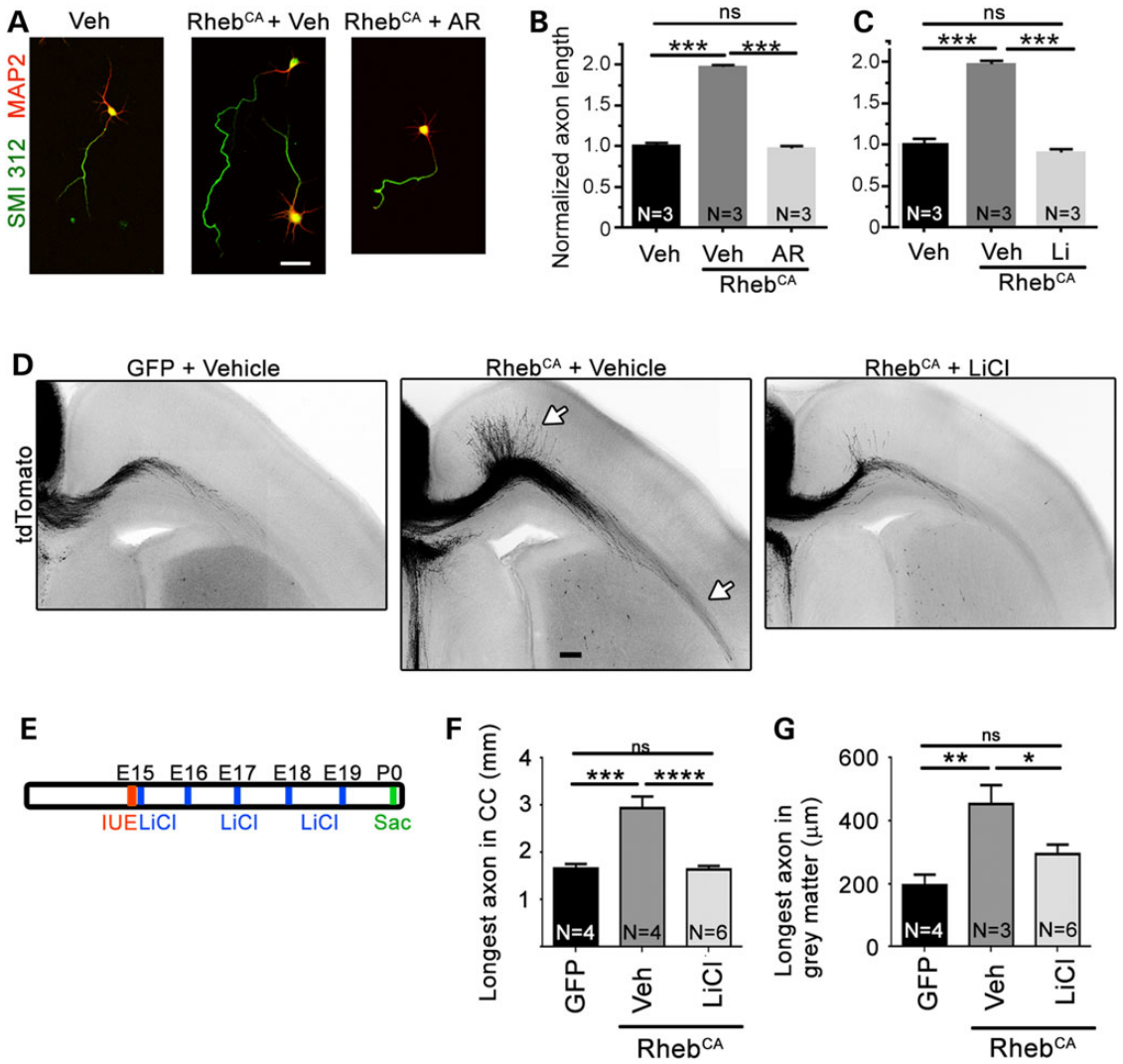

Figure 8. Blocking GSK3β with lithium chloride prevents accelerated axon growth induced by hyperactive mTORC1 *in vivo*. (**A**) Confocal images of tdTomato-nucleofected (data not shown) and BFP- or Rheb^{CA}-nucleofected cortical neurons immunostained for SMI 312 (green) and MAP2 (red) and treated with vehicle, AR-A014418 or LiCl. Scale bar: 40 µm. (**B** and **C**) Bar graph of axon length for neurons in condition indicated under each bar graph. Statistics: the number of neuronal culture used per condition is indicated in each column. (**D**) Confocal images of tdTomato-fluorescent axonal projections from ACC neurons electroporated at E15 with GFP or Rheb^{CA} and treated with vehicle (saline) or lithium chloride (LiCl). The white arrows point to longer axons in gray and white matter in the Rheb^{CA} + vehicle condition. Scale bar: 100 µm. (**E**) Diagram of the experimental protocol. (**F** and **G**) Bar graphs of the longest axon length in the corpus callosum (CC, $n = 15$ axons, $N = 4$ mice in GFP + vehicle; $n = 16$ axons, $N = 4$ mice in Rheb^{CA} + vehicle, and $n = 24$ axons, $N = 6$ mice in Rheb^{CA} + LiCl) and gray matter ($n = 9$ axons, $N = 4$ mice in GFP + vehicle; $n = 15$ axons, $N = 4$ mice in Rheb^{CA} + vehicle and $n = 24$ axons, $N = 6$ mice in Rheb^{CA} + LiCl). *$P < 0.05$, **$P < 0.01$ and ***$P < 0.001$, ****$P < 0.0001$ with one-way ANOVA and Tukey *post hoc* test; ns: not significant.

paraformaldehyde for 15 min and then incubated with primary antibody followed by the appropriate secondary antibody. Lithium (Sigma) and AR-A014418 (Sigma) were added to neuronal maintenance media 4 h after initial medium change.

Neuro2a cell culture and transfection

The Neuro2a mouse neuroblastoma cells were propagated using standard protocol and transfected with Polyjet (SignaGen Laboratories) at 80% confluence. Protein was harvested 48 or 72 h after transfection.

Western blots from mice, Neuro2a cells and nucleofected neurons

Neuro2a cells and neurons cultured for 6 days were lysed on ice using a lysis buffer consisting of radioimmunoprecipitation assay buffer, 1× Halt protease and phosphatase inhibitor (Thermo Scientific), 5 mM ethylenediaminetetraacetic acid and 20 units/ml DNase I (Roche). Lysates were cleared by spinning at 12 000 rcf for 10 min and then boiled with Laemmli sample buffer for 5 min. Lysates were run on 4–15% Tris–glycine gradient gels (Bio-rad, 456-1086) and transferred to polyvinylidene fluoride (PVDF) membranes. Membranes were then placed in blocking buffer (5% milk or 5% bovine serum albumin in tris-buffered saline (TBS) + 0.1% Tween 20) for 1 h at room temperature, followed by incubation with primary antibody in blocking buffer overnight at 4°C. Membranes were washed with TBS + 0.1% Tween 20 before another blocking buffer incubation followed by secondary antibody incubation at room temperature for 1 h. Antibodies are listed in Supplementary Material, Table S1.

Quantifications were performed using National Institutes of Health Image J software. Measurements were normalized to ERK as a loading control. For the phosphorylated form of proteins, data were normalized to the total levels from the same PVDF membrane.

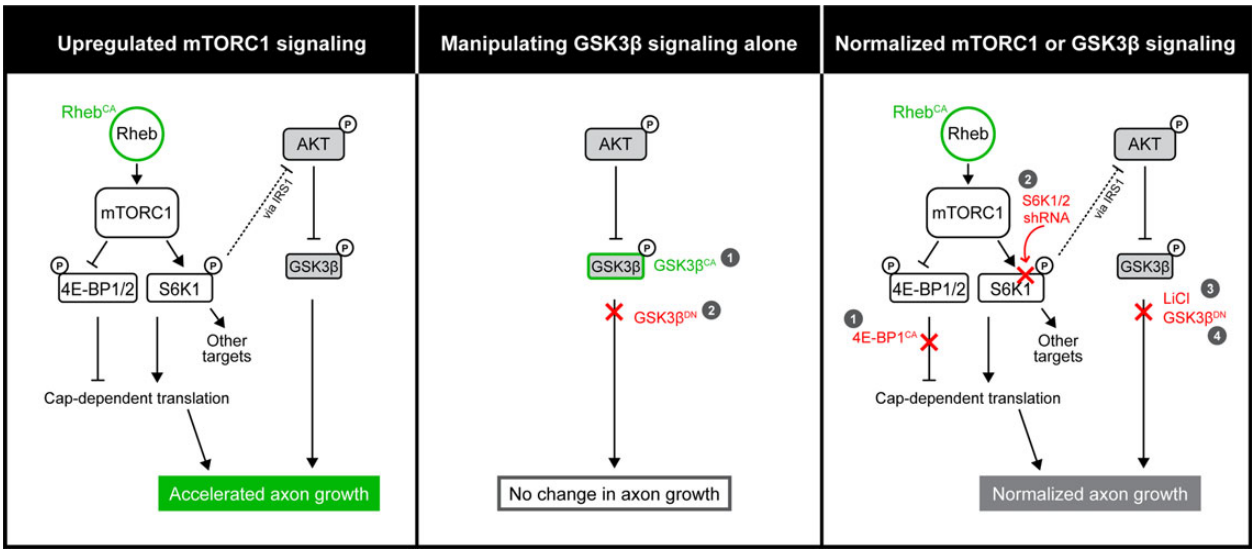

Figure 9. Diagram summarizing the Rheb-mTOR signaling pathway and findings presented in this study.

Quantification of axon length *in vivo* and *in vitro* and cell misplacement

Images of tdTomato+ axons were acquired in cultures or 150 and 100 μm thick coronal sections for axon length and misplacement analysis, respectively, using a Fluoview 1000 confocal microscope with a ×20 or ×10 objective. The length of the longest axon was measured both *in vitro* and *in vivo* because this was the most straightforward method and was similar to the one used *in vitro* by many others. *In vivo*, the axon length was measured from the midline to the tip of the longest axon. In addition, Z-stack images were acquired with the ×20 objective (with ×2 zoom) focusing at the tip of the axons to detect the longest axon. We measured in two to four consecutive sections per mouse and in $N > 3$ mice per condition because the longest axons could be cut in a single section. Axon length was measured using ImageJ at P0.

Cell misplacement was analyzed in P8 sections. The cortex was partitioned into 10 bins. Bins were evenly spaced from the pial surface to the white matter, with Bin 1 being the most superficial. The number of tdTomato+ cells in each bin was counted using the Cell Counter plugin for ImageJ. Only cells within the gray matter of the cortex were quantified.

All analyses were performed in sections with similar electroporation efficiency. To assess efficiency, the fluorescence intensity of the electroporated ACC was assessed in Image J to yield a mean ± standard deviation (SD) using sections shown in Figure 1. Every image was taken using a high-low filter to equalize fluorescence emission between sections. We analyzed axon length in sections that displayed a fluorescence intensity in the range of mean ± SD.

Drugs

AR-A014418 and lithium chloride were from Sigma–Aldrich. Rapamycin was from A.G. Scientific. All three drugs were dissolved in dimethyl sulfoxide (DMSO) (vehicle) for *in vitro* experiments and control cells were treated with similar concentrations of DMSO. For *in vivo* drug treatment, intraperitoneal injection of 600 mM LiCl or NaCl (10 μl/g body weight, saline) was performed every day from E15 after electroporation to E19 (64).

Statistics

N indicates the number of animals in each condition or the number of culture set. Data were plotted in GraphPad Prism 6. Statistical significance was determined using unpaired two-tailed Student's *t*-test or one-way analysis of variance (ANOVA) with Tukey *post hoc* test or two-way repeated-measures ANOVA with $P < 0.05$ for significance. Data are presented as mean ± standard error of the mean (SEM).

Supplementary Material

Supplementary Material is available at *HMG* online.

Acknowledgements

We thank Drs Hanada and Maehama (Tokyo) and J. Breunig for providing the Rheb^{CA} and BFP vectors, respectively, and Dr Sestan for providing access to the Amaxa nucleofector.

Conflict of Interest statement. None declared.

Funding

This work was supported by National Institutes of Health (R01 NS086329), McKnight Endowment Fund for Neuroscience award (A.B.) and training grants from the China Scholarship Council (X.G., T.H. and L.Z.).

References

1. Wong, M. (2013) Mammalian target of rapamycin (mTOR) pathways in neurological diseases. *Biomed. J.*, **36**, 40–50.
2. Ameis, S.H. and Catani, M. (2015) Altered white matter connectivity as a neural substrate for social impairment in Autism Spectrum Disorder. *Cortex*, **62**, 158–181.
3. Fornito, A. and Bullmore, E.T. (2014) Reconciling abnormalities of brain network structure and function in schizophrenia. *Curr. Opin. Neurobiol.*, **30**, 44–50.

4. Lasarge, C.L. and Danzer, S.C. (2014) Mechanisms regulating neuronal excitability and seizure development following mTOR pathway hyperactivation. *Front. Mol. Neurosci.*, **7**, 18.
5. Morita, T. and Sobue, K. (2009) Specification of neuronal polarity regulated by local translation of CRMP2 and Tau via the mTOR-p70S6 K pathway. *J. Biol. Chem.*, **284**, 27734–27745.
6. Li, Y.H., Werner, H. and Puschel, A.W. (2008) Rheb and mTOR regulate neuronal polarity through Rap1B. *J. Biol. Chem.*, **283**, 33784–33792.
7. Choi, Y.J., Di Nardo, A., Kramvis, I., Meikle, L., Kwiatkowski, D. J., Sahin, M. and He, X. (2008) Tuberous sclerosis complex proteins control axon formation. *Genes Dev.*, **22**, 2485–2495.
8. Garami, A., Zwartkruis, F.J., Nobukuni, T., Joaquin, M., Roccio, M., Stocker, H., Kozma, S.C., Hafen, E., Bos, J.L. and Thomas, G. (2003) Insulin activation of Rheb, a mediator of mTOR/S6K/4E-BP signaling, is inhibited by TSC1 and 2. *Mol. Cell*, **11**, 1457–1466.
9. Inoki, K., Li, Y., Xu, T. and Guan, K.L. (2003) Rheb GTPase is a direct target of TSC2 GAP activity and regulates mTOR signaling. *Genes Dev.*, **17**, 1829–1834.
10. Kwiatkowski, D.J. and Manning, B.D. (2005) Tuberous sclerosis: a GAP at the crossroads of multiple signaling pathways. *Hum. Mol. Genet.*, **14**, R251–R258.
11. Ma, X.M. and Blenis, J. (2009) Molecular mechanisms of mTOR-mediated translational control. *Nat. Rev. Mol. Cell Biol.*, **10**, 307–318.
12. Yan, L., Findlay, G.M., Jones, R., Procter, J., Cao, Y. and Lamb, R. F. (2006) Hyperactivation of mammalian target of rapamycin (mTOR) signaling by a gain-of-function mutant of the Rheb GTPase. *J. Biol. Chem.*, **281**, 19793–19797.
13. Lafourcade, C.A., Lin, T.V., Feliciano, D.M., Zhang, L., Hsieh, L. S. and Bordey, A. (2013) Rheb activation in subventricular zone progenitors leads to heterotopia, ectopic neuronal differentiation, and rapamycin-sensitive olfactory micronodules and dendrite hypertrophy of newborn neurons. *J. Neurosci.*, **33**, 2419–2431.
14. Hartman, N.W., Lin, T.V., Zhang, L., Paquelet, G.E., Feliciano, D.M. and Bordey, A. (2013) mTORC1 targets the translational repressor 4E-BP2, but not S6 kinase 1/2, to regulate neural stem cell self-renewal in vivo. *Cell Rep.*, **5**, 433–444.
15. Magnuson, B., Ekim, B. and Fingar, D.C. (2012) Regulation and function of ribosomal protein S6 kinase (S6K) within mTOR signalling networks. *Biochem. J.*, **441**, 1–21.
16. Meyuhas, O. and Dreazen, A. (2009) Ribosomal protein S6 kinase from TOP mRNAs to cell size. *Prog. Mol. Biol. Transl. Sci.*, **90**, 109–153.
17. Meikle, L., Pollizzi, K., Egnor, A., Kramvis, I., Lane, H., Sahin, M. and Kwiatkowski, D.J. (2008) Response of a neuronal model of tuberous sclerosis to mammalian target of rapamycin (mTOR) inhibitors: effects on mTORC1 and Akt signaling lead to improved survival and function. *J. Neurosci.*, **28**, 5422–5432.
18. Carson, R.P., Van Nielen, D.L., Winzenburger, P.A. and Ess, K. C. (2012) Neuronal and glia abnormalities in Tsc1-deficient forebrain and partial rescue by rapamycin. *Neurobiol. Dis.*, **45**, 369–380.
19. Zhang, H.H., Lipovsky, A.I., Dibble, C.C., Sahin, M. and Manning, B.D. (2006) S6K1 regulates GSK3 under conditions of mTOR-dependent feedback inhibition of Akt. *Mol. Cell*, **24**, 185–197.
20. Kim, Y.T., Hur, E.M., Snider, W.D. and Zhou, F.Q. (2011) Role of GSK3 signaling in neuronal morphogenesis. *Front. Mol. Neurosci.*, **4**, 48.
21. Seira, O. and Del Rio, J.A. (2014) Glycogen synthase kinase 3 beta (GSK3beta) at the tip of neuronal development and regeneration. *Mol. Neurobiol.*, **49**, 931–944.
22. Hur, E.M. and Zhou, F.Q. (2010) GSK3 signalling in neural development. *Nat. Rev. Neurosci.*, **11**, 539–551.
23. Zhang, L., Bartley, C.M., Gong, X., Hsieh, L.S., Lin, T.V., Feliciano, D.M. and Bordey, A. (2014) MEK-ERK1/2-dependent FLNA overexpression promotes abnormal dendritic patterning in tuberous sclerosis independent of mTOR. *Neuron*, **84**, 78–91.
24. Maehama, T., Tanaka, M., Nishina, H., Murakami, M., Kanaho, Y. and Hanada, K. (2008) RalA functions as an indispensable signal mediator for the nutrient-sensing system. *J. Biol. Chem.*, **283**, 35053–35059.
25. Ridler, K., Suckling, J., Higgins, N.J., de Vries, P.J., Stephenson, C.M., Bolton, P.F. and Bullmore, E.T. (2007) Neuroanatomical correlates of memory deficits in tuberous sclerosis complex. *Cereb. Cortex*, **17**, 261–271.
26. Zikopoulos, B. and Barbas, H. (2013) Altered neural connectivity in excitatory and inhibitory cortical circuits in autism. *Front. Hum. Neurosci.*, **7**, 609.
27. Yasuda, S., Sugiura, H., Katsurabayashi, S., Shimada, T., Tanaka, H., Takasaki, K., Iwasaki, K., Kobayashi, T., Hino, O. and Yamagata, K. (2014) Activation of Rheb, but not of mTORC1, impairs spine synapse morphogenesis in tuberous sclerosis complex. *Sci. Rep.*, **4**, 5155.
28. Choi, K.M., McMahon, L.P. and Lawrence, J.C. Jr (2003) Two motifs in the translational repressor PHAS-I required for efficient phosphorylation by mammalian target of rapamycin and for recognition by raptor. *J. Biol. Chem.*, **278**, 19667–19673.
29. Schalm, S.S. and Blenis, J. (2002) Identification of a conserved motif required for mTOR signaling. *Curr. Biol.*, **12**, 632–639.
30. Lucas, F.R., Goold, R.G., Gordon-Weeks, P.R. and Salinas, P.C. (1998) Inhibition of GSK-3beta leading to the loss of phosphorylated MAP-1B is an early event in axonal remodelling induced by WNT-7a or lithium. *J. Cell Sci.*, **111**, 1351–1361.
31. Goold, R.G., Owen, R. and Gordon-Weeks, P.R. (1999) Glycogen synthase kinase 3beta phosphorylation of microtubule-associated protein 1B regulates the stability of microtubules in growth cones. *J. Cell Sci.*, **112**, 3373–3384.
32. Hagen, T., Di, D.E., Culbert, A.A. and Reith, A.D. (2002) Expression and characterization of GSK-3 mutants and their effect on beta-catenin phosphorylation in intact cells. *J. Biol. Chem.*, **277**, 23330–23335.
33. Liz, M.A., Mar, F.M., Santos, T.E., Pimentel, H.I., Marques, A.M., Morgado, M.M., Vieira, S., Sousa, V.F., Pemble, H., Wittmann, T. *et al.* (2014) Neuronal deletion of GSK3beta increases microtubule speed in the growth cone and enhances axon regeneration via CRMP-2 and independently of MAP1B and CLASP2. *BMC Biol.*, **12**, 47.
34. Gartner, A., Huang, X. and Hall, A. (2006) Neuronal polarity is regulated by glycogen synthase kinase-3 (GSK-3beta) independently of Akt/PKB serine phosphorylation. *J. Cell Sci.*, **119**, 3927–3934.
35. Feliciano, D.M., Su, T., Lopez, J., Platel, J.C. and Bordey, A. (2011) Single-cell Tsc1 knockout during corticogenesis generates tuber-like lesions and reduces seizure threshold in mice. *J. Clin. Invest*, **121**, 1596–1607.
36. Tsai, V., Parker, W.E., Orlova, K.A., Baybis, M., Chi, A.W., Berg, B.D., Birnbaum, J.F., Estevez, J., Okochi, K., Sarnat, H.B. *et al.* (2014) Fetal brain mTOR signaling activation in tuberous sclerosis complex. *Cereb. Cortex*, **24**, 315–327.
37. Kassai, H., Sugaya, Y., Noda, S., Nakao, K., Maeda, T., Kano, M. and Aiba, A. (2014) Selective activation of mTORC1 signaling

recapitulates microcephaly, tuberous sclerosis, and neurodegenerative diseases. *Cell Rep.*, **7**, 1626–1639.
38. Cohen, P. and Goedert, M. (2004) GSK3 inhibitors: development and therapeutic potential. *Nat. Rev. Drug Discov.*, **3**, 479–487.
39. Gould, T.D., Einat, H., Bhat, R. and Manji, H.K. (2004) AR-A014418, a selective GSK-3 inhibitor, produces antidepressant-like effects in the forced swim test. *Int. J. Neuropsychopharmacol.*, **7**, 387–390.
40. Zhou, J., Blundell, J., Ogawa, S., Kwon, C.H., Zhang, W., Sinton, C., Powell, C.M. and Parada, L.F. (2009) Pharmacological inhibition of mTORC1 suppresses anatomical, cellular, and behavioral abnormalities in neural-specific Pten knock-out mice. *J. Neurosci.*, **29**, 1773–1783.
41. Abe, N., Borson, S.H., Gambello, M.J., Wang, F. and Cavalli, V. (2010) Mammalian target of rapamycin (mTOR) activation increases axonal growth capacity of injured peripheral nerves. *J. Biol. Chem.*, **285**, 28034–28043.
42. Park, K.K., Liu, K., Hu, Y., Smith, P.D., Wang, C., Cai, B., Xu, B., Connolly, L., Kramvis, I., Sahin, M. *et al.* (2008) Promoting axon regeneration in the adult CNS by modulation of the PTEN/mTOR pathway. *Science*, **322**, 963–966.
43. Liu, K., Lu, Y., Lee, J.K., Samara, R., Willenberg, R., Sears-Kraxberger, I., Tedeschi, A., Park, K.K., Jin, D., Cai, B. *et al.* (2010) PTEN deletion enhances the regenerative ability of adult corticospinal neurons. *Nat. Neurosci.*, **13**, 1075–1081.
44. Harrington, L.S., Findlay, G.M. and Lamb, R.F. (2005) Restraining PI3K: mTOR signalling goes back to the membrane. *Trends Biochem. Sci.*, **30**, 35–42.
45. Shah, O.J. and Hunter, T. (2005) Tuberous sclerosis and insulin resistance. Unlikely bedfellows reveal a TORrid affair. *Cell Cycle*, **4**, 46–51.
46. Um, S.H., D'Alessio, D. and Thomas, G. (2006) Nutrient overload, insulin resistance, and ribosomal protein S6 kinase 1, S6K1. *Cell Metab.*, **3**, 393–402.
47. Doble, B.W. and Woodgett, J.R. (2003) GSK-3: tricks of the trade for a multi-tasking kinase. *J. Cell Sci.*, **116**, 1175–1186.
48. Zhou, F.Q., Zhou, J., Dedhar, S., Wu, Y.H. and Snider, W.D. (2004) NGF-induced axon growth is mediated by localized inactivation of GSK-3beta and functions of the microtubule plus end binding protein APC. *Neuron*, **42**, 897–912.
49. Jiang, H., Guo, W., Liang, X. and Rao, Y. (2005) Both the establishment and the maintenance of neuronal polarity require active mechanisms: critical roles of GSK-3beta and its upstream regulators. *Cell*, **120**, 123–135.
50. Yoshimura, T., Kawano, Y., Arimura, N., Kawabata, S., Kikuchi, A. and Kaibuchi, K. (2005) GSK-3beta regulates phosphorylation of CRMP-2 and neuronal polarity. *Cell*, **120**, 137–149.
51. Kim, W.Y., Zhou, F.Q., Zhou, J., Yokota, Y., Wang, Y.M., Yoshimura, T., Kaibuchi, K., Woodgett, J.R., Anton, E.S. and Snider, W.D. (2006) Essential roles for GSK-3s and GSK-3-primed substrates in neurotrophin-induced and hippocampal axon growth. *Neuron*, **52**, 981–996.
52. Garrido, J.J., Simon, D., Varea, O. and Wandosell, F. (2007) GSK3 alpha and GSK3 beta are necessary for axon formation. *FEBS Lett.*, **581**, 1579–1586.
53. Alabed, Y.Z., Pool, M., Ong, T.S., Sutherland, C. and Fournier, A.E. (2010) GSK3 beta regulates myelin-dependent axon outgrowth inhibition through CRMP4. *J. Neurosci.*, **30**, 5635–5643.
54. Hur, E.M., Saijilafu, Lee, B.D., Kim, S.J., Xu, W.L. and Zhou, F.Q. (2011) GSK3 controls axon growth via CLASP-mediated regulation of growth cone microtubules. *Genes Dev.*, **25**, 1968–1981.
55. Owen, R. and Gordon-Weeks, P.R. (2003) Inhibition of glycogen synthase kinase 3beta in sensory neurons in culture alters filopodia dynamics and microtubule distribution in growth cones. *Mol. Cell Neurosci.*, **23**, 626–637.
56. Li, C.L., Sathyamurthy, A., Oldenborg, A., Tank, D. and Ramanan, N. (2014) SRF phosphorylation by glycogen synthase kinase-3 promotes axon growth in hippocampal neurons. *J. Neurosci.*, **34**, 4027–4042.
57. Cole, A.R., Knebel, A., Morrice, N.A., Robertson, L.A., Irving, A.J., Connolly, C.N. and Sutherland, C. (2004) GSK-3 phosphorylation of the Alzheimer epitope within collapsin response mediator proteins regulates axon elongation in primary neurons. *J. Biol. Chem.*, **279**, 50176–50180.
58. Burbridge, T.J., Xu, H.P., Ackman, J.B., Ge, X., Zhang, Y., Ye, M.J., Zhou, Z.J., Xu, J., Contractor, A. and Crair, M.C. (2014) Visual circuit development requires patterned activity mediated by retinal acetylcholine receptors. *Neuron*, **84**, 1049–1064.
59. Lim, K.C. and Crino, P.B. (2013) Focal malformations of cortical development: new vistas for molecular pathogenesis. *Neuroscience*, **252**, 262–276.
60. Lim, J.S., Kim, W.I., Kang, H.C., Kim, S.H., Park, A.H., Park, E.K., Cho, Y.W., Kim, S., Kim, H.M., Kim, J.A. *et al.* (2015) Brain somatic mutations in MTOR cause focal cortical dysplasia type II leading to intractable epilepsy. *Nat. Med.*, **21**, 395–400.
61. Bae, E.J., Xu, J., Oh, D.Y., Bandyopadhyay, G., Lagakos, W.S., Keshwani, M. and Olefsky, J.M. (2012) Liver-specific p70 S6 kinase depletion protects against hepatic steatosis and systemic insulin resistance. *J. Biol. Chem.*, **287**, 18769–18780.
62. Ventura, A., Meissner, A., Dillon, C.P., McManus, M., Sharp, P.A., Van Parijs, L., Jaenisch, R. and Jacks, T. (2004) Cre-lox-regulated conditional RNA interference from transgenes. *Proc. Natl Acad. Sci. USA*, **101**, 10380–10385.
63. Pathania, M., Torres-Reveron, J., Yan, L., Kimura, T., Lin, T.V., Gordon, V., Teng, Z.Q., Zhao, X., Fulga, T.A., Van, V.D. *et al.* (2012) miR-132 enhances dendritic morphogenesis, spine density, synaptic integration, and survival of newborn olfactory bulb neurons. *PLoS One*, **7**, e38174.
64. Lancaster, M.A., Gopal, D.J., Kim, J., Saleem, S.N., Silhavy, J.L., Louie, C.M., Thacker, B.E., Williams, Y., Zaki, M.S. and Gleeson, J.G. (2011) Defective Wnt-dependent cerebellar midline fusion in a mouse model of Joubert syndrome. *Nat. Med.*, **17**, 726–731.